Polyaniline globules as a catalyst for WO3 nanoparticles for supercapacitor application

To cite this article before publication: Anamika Vitthal Kadam *et al* 2018 *Mater. Res. Express* in press https://doi.org/10.1088/2053-1591/aad406

Polyaniline globules as a catalyst for WO_3 nanoparticles for supercapacitor application

Anamika V. Kadam, Shubham Patil

D.Y. Patil College of Engineering and Technology, Kasaba Bawada, Kolhapur-416006, Maharashtra, India, email address-anamikasonavane@rediff.com, https://orcid.org/0000-0003-1514-9337

Abstract

Microglobules of polyaniline (PANi) synthesized by chemical bath method on commercial steel plates that have been used as the catalyst support for tungsten trioxide (WO_3) particles fabricated by hydrothermal method. The crystalline phases and surface analysis of the WO_3, PANi and WO_3/PANi film were examined using X-ray diffraction and scanning electron microscopy, while electrochemical capacitive properties were determined using cyclic voltammetry (CV), electrochemical impedance spectroscopy (EIS) and galvanostatic charge-discharge (GCD). The PANi incorporated WO_3 film influences significant catalytic performance wherein a pseudo-capacitor was obtained. The constant phase element was considerably eliminated in WO_3/PANi hybrid film. The cyclic stability was scrutinized via GCD technique. The degradation of specific capacitance observed low (2.61%) after 3000 GCD cycles, indicating superior cycling stability of WO_3/PANi supercapacitor.

Keywords: polyaniline, tungsten trioxide, supercapacitor, catalyst

1. Introduction

Present studies on various pseudo-capacitive materials are mostly based on transition metal oxides [1]. Due to simple synthesis, outstanding conductivity, high capacity, and universality, WO_3 is the best electrode material for supercapacitor [2]. In n-type of semiconductor, WO_3 has the best corrosion resistance and excellent electron transport properties [3-4] WO_3 nanofiber has offered the lowest internal resistance revealing highest

conductivity [5]. Qiu et al. adopted electrodeposition technique to synthesize n-type flowerlike WO_3 electrode for all-solid-state asymmetric supercapacitors and shown an effective electrochemical behavior of 196 F g^{-1} at a sweep rate of 10 mV/s [6, 7]. However, hydrothermally grown hierarchical WO_3 nanofibers enriched on carbon clothes gives an excellent performance of cyclability, specific capacity, initial discharge capacitance and stability [7]. Besides metal oxides, conducting polymers have concerned interests in energy storage, sensors and electrochromic devices [8-10]. They have high conductivity and excellent capacitive properties [11]. Elements in it like C, H, N or S also indicates the high affordability [12]. In connection with several conducting polymers, polyaniline (PANi) has encountered most attention on account of its highest specific capacitance owing to multi-redox reactions, good electronic properties due to protonation [11], improved thermal stability including reasonable cost [13-14]. It can simply be blended in a form of thin film or powder by chemically or electrochemically deposition method [15]. In light of these beneficial properties, PANi has been long-established in energy storage and conversion devices, containing supercapacitors [16], batteries [17] and fuel cells [18]. In case of PANi as a supercapacitor, it accumulates the charge by redox reaction on account of its various oxidation states with a maximum specific capacity about 950 Fg^{-1} [16, 19].

The incorporation of PANi inside tungsten trioxide gives rise to promising applications such as gas sensor [20], supercapacitor [21-22], humidity sensor [23], electrochromic energy storage [24-25], catalyst [26] and so on. Among these, the advancement of a supercapacitor in energy storage application has received adequate attention. Particularly, the advantage of WO_3/PANi composite promoted the degree of equivalence in ion transfer characteristics of both the materials [27-30]. In addition, doping of PANi has been recognized as a promising catalyst in various applications [31-32] that facilitates electronic conductivity, oxygen mass transfer, corrosion resistance, durability.

Although WO_3/PANi composites have been assembled by adopting several techniques; nevertheless, the efficacy of these materials explored less in all the circumstances.

To date several methods have been used to fabricate WO_3/PANi thin film for supercapacitor characteristics including potentio-dynamic co-deposition [33], chemical synthesis on WO_3 prepared via chemical bath deposition [34], potentio-dynamic deposition via sol-gel method [35], galvanostatic electrodeposition on chemically prepared WO_3 [36]. Thus, from the literature survey, it clearly indicates that there was no research on hydrothermally grown tungsten oxide film with PANi for supercapacitor application. Hence, the present work was planned to deposit WO_3 by hydrothermal method. In the second part, PANi was coated on WO_3 by chemical bath deposition.

2. Experimental section

2.1.Preparation of steel substrates:

To improve the substrate profile, initially, a large square of steel plate cut in the 3.5x1 cm^2 area with A grade quality blade. Further alkaline cleaning of steel substrates provided to remove contaminant followed by heat treatment (60°C) in a solution of nitric acid (25% by weight) and double distilled water, ddH_2O (75% by weight) for 20 minutes. The substrates were cleaned with plain ddH_2O and dried in air. Thus, steel substrates prepared for the deposition process.

2.2. Materials

All the chemicals were of analytical grade and taken without further purification or modification. Tungstic acid (H_2WO_4) is the starting material. Hydrochloric acid (HCl), hydrogen peroxide (H_2O_2), ethylene glycol $(CH_2OH)_2$, aniline ($C_6H_5NH_2$) and ammonium per sulphate ($(NH_4)_2S_2O_8$) were the other chemicals used for the growth of WO_3/PANi film.

2.3. Fabrication of WO_3 films

In a typical procedure, 2.5g of H_2WO_4 was dissolved in 30 mL of H_2O_2 and diluted to 100 mL by ddH_2O. Out of the above solution, in 10 mL solution, 3.5 mL of 3 M HCl added dropwise and stirred continuously. While stirring the solution, 25 mL of $(CH_2OH)_2$ added to the precursor vigorously. Further, the solution was poured in an autoclave (40 mL Teflon-lined stainless steel vessel) with a cleaned substrate and preserved at 180 °C for 90 min. The as-obtained films were cooled at room temperature and annealed at 400 °C for 2h in the furnace. Thus annealed WO_3 films on steel substrates were prepared.

2.4. Fabrication of WO_3/PANi films:

In the second part of experiment, PANi solution was prepared by adding 2 mL of aniline in 30mL of 1 M HCl solution in one beaker and 1.95 g ($(NH_4)_2S_2O_8$) and 20mL of 1 M HCl in the other beaker. These two solutions were added separately in an empty beaker by maintaining the temperature at 5°C. Thus PANi solution is prepared for the deposition process. Further, the bare steel substrates (to deposit PANi film) and annealed WO_3 films (to deposit WO_3/PANi film) were dipped in PANi solution twice for 10 sec and dried at room temperature. Consequently, PANi, WO_3 and WO_3/PANi films were prepared on the steel substrates for further characterization.

2.5. Characterization Techniques:

The morphologies of WO_3, PANi and WO_3/PANi films were characterized using scanning electron microscopy (SEM, Hitachi S-4700 II, 25 kV). The crystal patterns were obtained via X-ray diffraction (XRD, Thermo ARLSCINTAG X'TRA with copper K_α irradiation, λ = 0.154056 nm). Electrochemical behavior and capacitance determinations were carried out in a classical three electrode set-ups using cyclic voltammetry (CV) and Nyquist plot on a CHI608E electrochemical analyzer with 0.5 M $LiClO_4$-PC electrolyte. For this, the

nanotablets on the metal substrates were used as a working electrode; graphite plate served as a counter electrode and a standard calomel electrode (SCE) electrode served as a reference electrode. Further Nyquist curves were simulated using software (ZSimpWin 3.21).

3 Results and discussion:

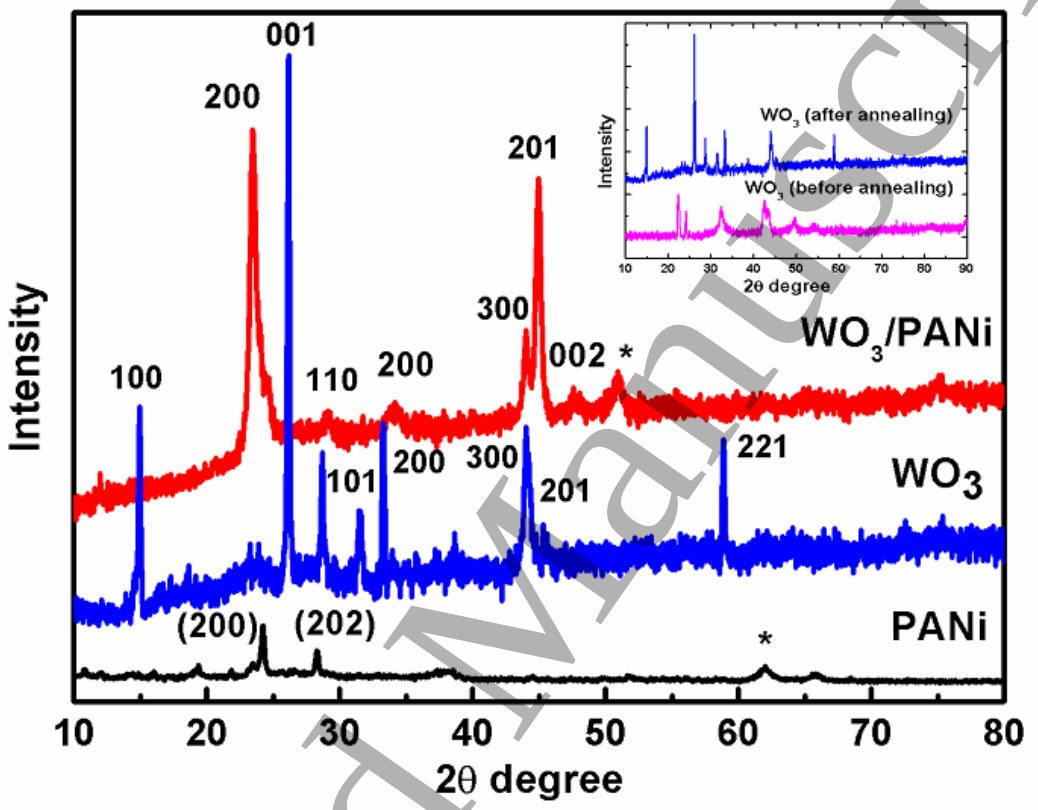

Fig. 1: XRD patterns of WO_3, PANi, WO_3/PANi samples where asterisk (*) denotes peaks of steel substrate. The inset shows XRD patterns of before and after annealed WO_3 samples

The XRD corroborated the crystal phases of all the samples depicted in fig.1. It indicates the orthorhombic structure of as-prepared tungsten trioxide (WO_3, JCPDS card 20-1324), wherein the broad peaks and amorphous hump in the pattern show poor crystallinity. The annealed WO_3 sample displayed a pure hexagonal structure (JCPDS card 33-1387) with the elimination of other peaks (shown in inset of Fig. 1). Pure PANi film has the partial crystalline orthorhombic C_6H_7N structure (JCPDS file 00-053-1718) [37, 38]. However, in WO_3/PANi only two diffraction peaks were obtained, one owing to the PANi peak (at 2θ=23°) [38] and the other peaks of WO_3 (2θ located at 29°, 34°, 43°, 45° and 47°) [39]. The

other diffraction peaks were slightly seen in WO_3/PANi sample on account of the protonic acid doping of PANi that recrystallizes WO_3. The steel substrate peaks are denoted by asterisk (*) [40].

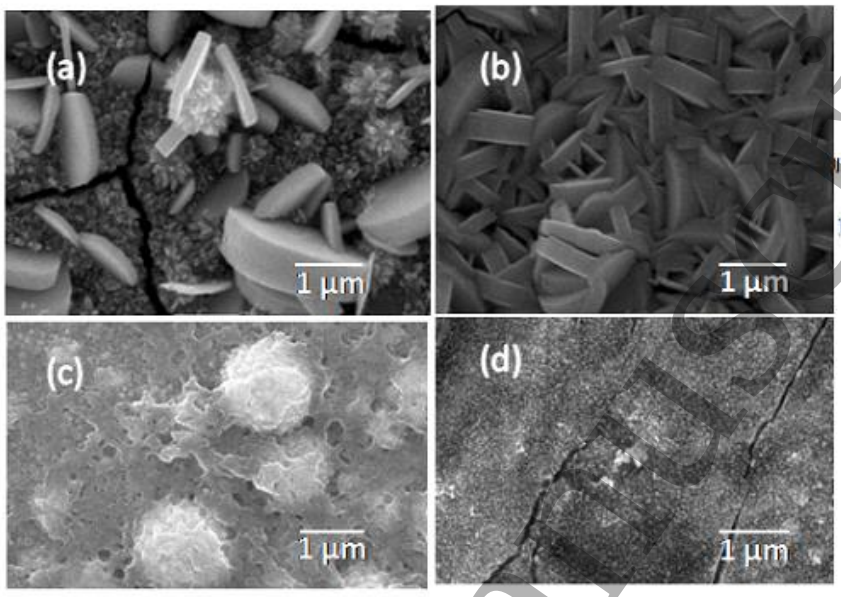

Fig. 2: Scanning Electron Microscope (SEM) images of (a,b) WO_3 samples (before, after annealed), (c) PANi and (d) WO_3/PANi hybrid sample

Fig. 2 shows the SEM images of synthesized WO_3 thin films before and after annealing (a, b), PANi (c) and a composite WO_3/PANi (d) respectively. As prepared sample showed cracked morphology with randomly distributed micro-sized tablet shaped particles with poor uniformity on the surface (Fig. 1 (a)), Whereas annealed WO_3 sample revealed a uniform nanotablet like morphology (Fig.1(b)). The average size of the nanotablets was of the order of 100-250 nm in width and 800-1000 nm in length. PANi film displayed globular morphology (fig. 1 (c)). When PANi coated on annealed WO_3 film, it was observed that the nanotablet melted under the effect of PANi, keeping the residue of uniformly distributed nanodot on the surface of the substrate. The sizes of nanodot were of the order of 100 nm with nanoporous structure (fig. 1 (d)). As a result, PANi provided quantum confinement effect to WO_3.

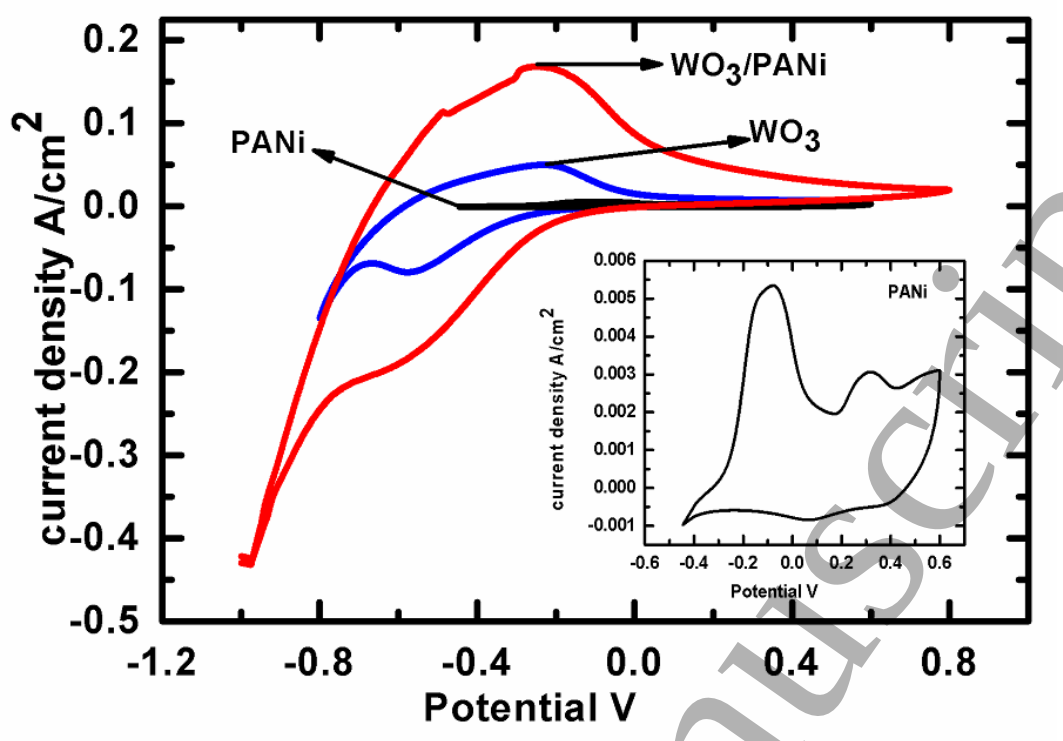

Fig. 3: Cyclic voltammogram records of WO_3, PANi and WO_3/PANi hybrid in 0.5 M $LiClO_4$-PC electrolyte at the scanning rate 100 mV/s. The inset represents CV of PANi sample.

Table 1: Charge storage properties of the samples

Sample ↓	Charge-discharge				Cyclic Voltammetry			
	Potential window (V)	Current density (mA/cm^2)	Specific capacitance (mF/g)	Areal capacitance (mF/cm^2)	Potential window (V)	Sweep rate (mV/s)	Specific capacitance (mF/g)	Areal capacitance (mF/cm^2)
WO_3	0.0−0.8	0.5	908.1	5.11	-1−0.8	100	5.760	67
PANi	0.0−0.8	0.05	336.5	2.09	-0.45 −0.6	100	0.87	10
WO_3/PANi	0.0−0.8	0.05	774.4	5.19	-0.8 −0.6	100	21.37	294

Fig. 3 compares the cyclic voltammetric changes of the films recorded in 0.5 M $LiClO_4$-PC electrolyte in a potential window of -0.8 to 0.6 V, -0.5 to +0.6 V and -1.1 to +0.8 V for WO_3, PANi and WO_3/PANi films. PANi film displayed oxidation peak at approximately +0.6 V in

forwarding scan, though the oxidation of aniline was not clearly seen in the forward scan, the reverse scan shows a small shoulder at +0.3 and -0.1 V, which was due to the reduction of PANi formed on the electrode (inset of fig. 3). The WO_3 thin film showed a small oxidation and reduction peak at -0.6 and -0.3V vs SCE. However, WO_3/PANi film illustrated a large difference among the CV of PANi and WO_3. The enhancement of the peak current density of about 0.16 A/cm^2 could be observed in WO_3/PANi composite film with respect to pure PANi and WO_3 films and is comparable to the earlier reports [34]. This could be due to the nanoporous structure of WO_3/PANi which provided more reactive centers on the film to contact with the electrolyte and so assist the charge transfer process with improved charge density. This also indicated the catalytic behavior of PANi in WO_3.

The capacitance from CV curve of all the film calculated using following relation [34, 41]:

$C=I_{max}/ds$ where I_{max} is the maximum current (in Ampere) and ds is the potential scan rate in V/s. Further, the specific capacitance (C_s) and areal capacitance (C_a) was evaluated using the following equation and summarized in table 1:

C_s= C/m and C_a = C/A where m and A are the mass and area of deposited film dipped in an electrolyte. Mass of WO_3, PANi and WO_3/PANi films were measured using a high precision weight balance and is evaluated as 0.0117, 0.0117 and 0.0138 g respectively.

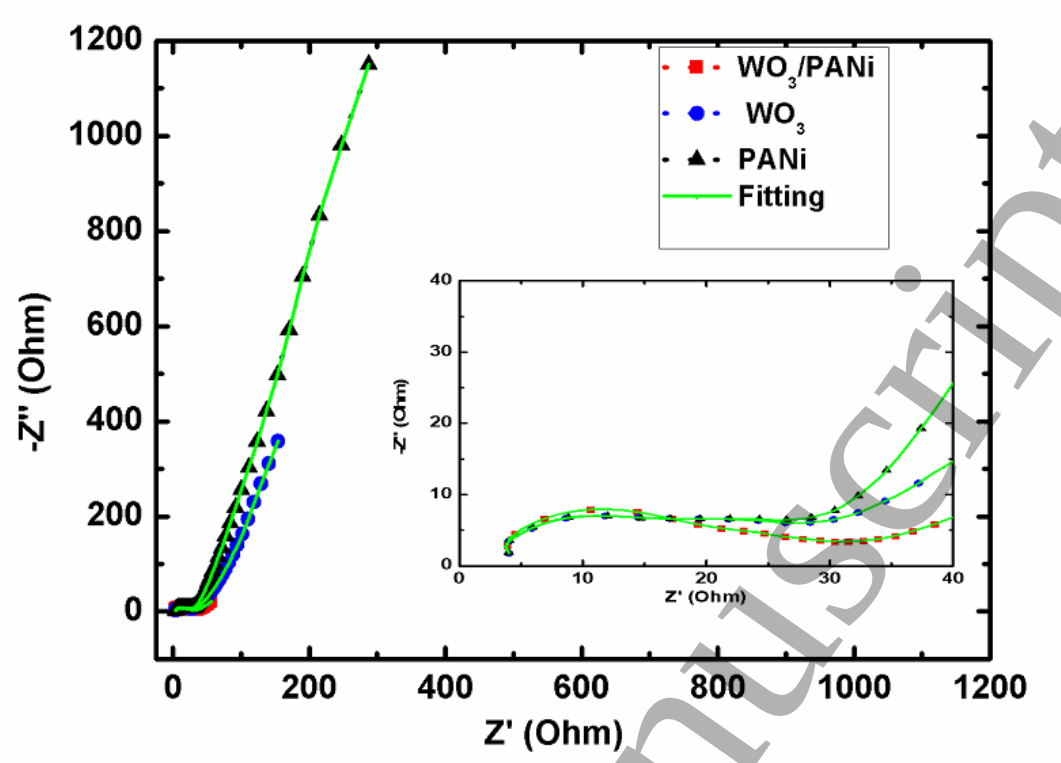

Fig. 4 : Typical Nyquist plots of WO_3, PANi and WO_3/PANi hybrid in 0.5 M $LiClO_4$-PC electrolyte with a frequency loop from 100 kHz to 1 Hz using open circuit potential of +0.38 V, +0.07 V and -0.4 V.

AC impedance spectra (EIS) of PANi, WO_3, and WO_3/PANi were measured to substantiate our approach of injecting PANi over WO_3 nanotablets using a hydrothermal method that contributed superior strength in electricity, ion diffusion process, and structural cyclability [42, 43]. Fig. 4 displayed the impedance spectra of a WO_3, PANi, and WO_3/PANi measured at +0.38V, +0.07V, and -0.4V respectively. Strikingly, the diffusion layer resistance of WO_3/PANi was lower than their sole performance. An impedance spectrum in the Nyquist plot possesses a straight line inclined by 45º at a higher frequency and a semicircle at a lower frequency. However, the compressed semicircle indicated irregular electrode surface that compensates double layer capacitance (C_{DL}) by a constant phase element (C_{PE}) [43]. Particularly, the Nyquist plot of WO_3/PANi exemplified small straight line at higher frequencies as a result of the diffusion process and a broad semicircle in the smaller frequency attributed to fast electron transfer and its prolonged existence in the film [43].

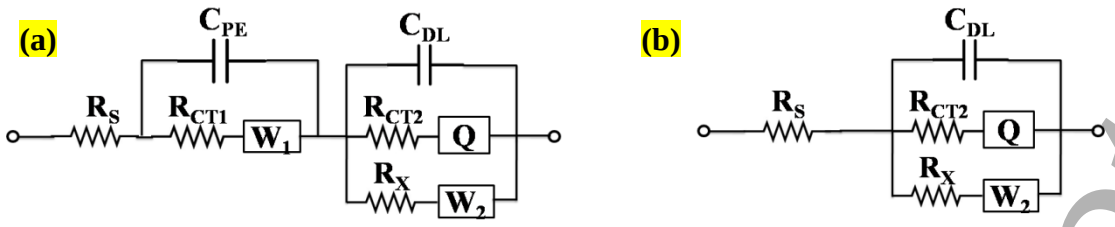

Fig. 5: Equivalent Randles circuit for (a) WO_3, PANi (b) WO_3/PANi hybrid used for fitting the experimental impedance plots obtained in fig. 4.

Table 2: Electrical parameters obtained using the Randles equivalent circuit of fig.5

Sample ↓	R_S (Ω)	R_{CT1} (Ω)	C_{PE} (μF)	W_1	R_{CT2} (Ω)	C_{DL} (μF)	R_X (Ω)	W_2
WO_3	3.308	10.23	11.3	0.00268	16.7	47.35	0.001	0.00023
PANi	3.227	0.028	124	0.00008	16.58	855.3	29	0.00230
WO_3/PANi	3.121	-----	-----	-----	31.09	668.3	25.03	0.00012

The corresponding Randles circuit shown in fig. 5 (a,b) included Rx, a resistance in parallel with R_{CT} (charge transfer resistance), to give a good fit to the experimental data summarized in table 2. W is the Warburg element indicating a comparable electrical component that replicates the diffusion process in the dielectric medium [44]. Warburg element (W) for PANi, WO_3, and WO_3/PANi observed as 0.002303, 0.0002313 and 0.0001214. These values elucidated that PANi improves the structural property of WO_3 facilitating good charge transport. In WO3/PANi (fig. 5b), C_{PE} was considerably eliminated that circumvent the flattening of the semicircle.

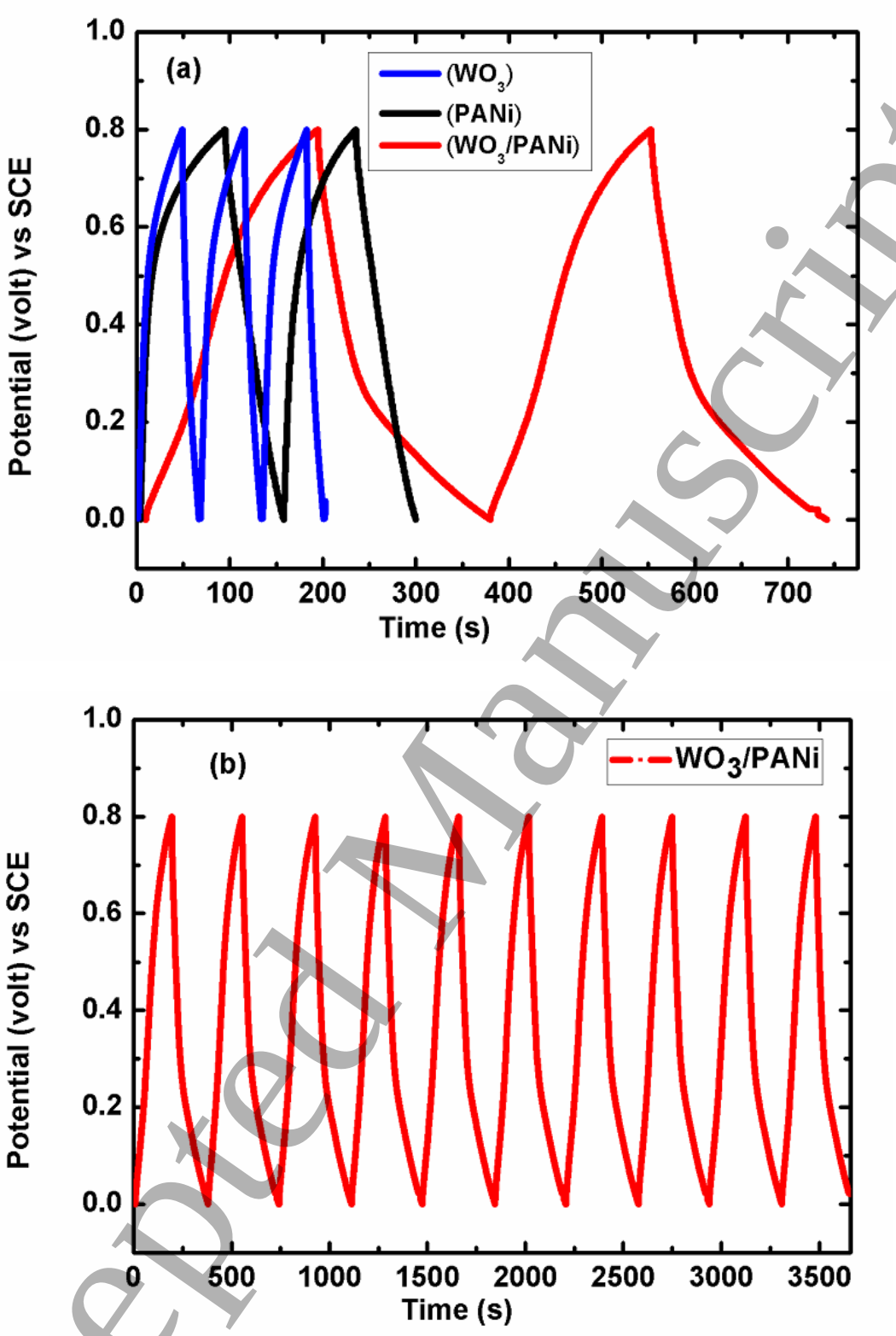

Fig. 6: (a) Galvanostatic charge/discharge (GCD) curve of WO_3, PANi and WO_3/PANi hybrid in 0.5 M $LiClO_4$-PC electrolyte at current density of 0.5, 0.05 and 0.05 mA/cm^2 respectively (b) GCD of WO3/PANi for initial 10 cycles

The galvanostatic charge-discharge (GCD) is a trustworthy technique to measure the electrochemical behavior of the material under controlled conditions using three electrode

systems with 0.5 M $LiClO_4$-PC electrolyte [45]. Fig. 6(a) exhibited GCD curves of PANi, WO_3, and WO_3/PANi for initial cycles at constant current density of 0.05, 0.5 and 0.05 mA/cm^2 respectively , while fig. 6(b) represents charge-discharge cycles for initial 10 cycles of WO_3/PANi films. The potential responses of the composite film during charge-discharge were more symmetrical than the sole performance of WO_3 and the working potential could be extended to 0.8 V. The discharge curve represented the characteristic profile of a pseudocapacitance showing the potential dependent nature of faradic reaction [46]. When we correlated GCD with the morphological study, it indicated that WO_3 has a larger particle size that decreases surface density increasing the interplanar spacing between atoms. Thus, during the charging process, it utilizes less coulombic force that accumulates large charges in a short time. Subsequently, the capacity of WO_3 increases with less charge-discharge time. In PANi, the charge-discharge time increases because it is highly conductive consisting of many electrons that enhances displacement of the electron cloud. Accordingly, it utilizes more coulombic force with the increase in charge-discharge time. However, when PANi coated over WO_3, it enhances the surface area of WO_3 with the reduction in the distance [47]. Ultimately the resistance decreases intrinsically with the improved charge transport process. Owing to this, WO_3/PANi uses more coulombic force with more time for charging and discharging process. Therefore, the charge storing capacity of the system enhances. The values of specific and areal capacitance enumerated in table 2. The results were consistent with EIS and XRD studies.

The capacitance from GCD curves evaluated using following relation [48, 49]:

$C= It_d/m\Delta V$ Where I and t_d are the in applied current density and time discharge, ΔV is the potential range, m is the mass of deposited film mentioned above. From this value of capacitance, the specific capacitance (F/g) and areal capacitance (F/cm^2) were measured and presented in table 1.

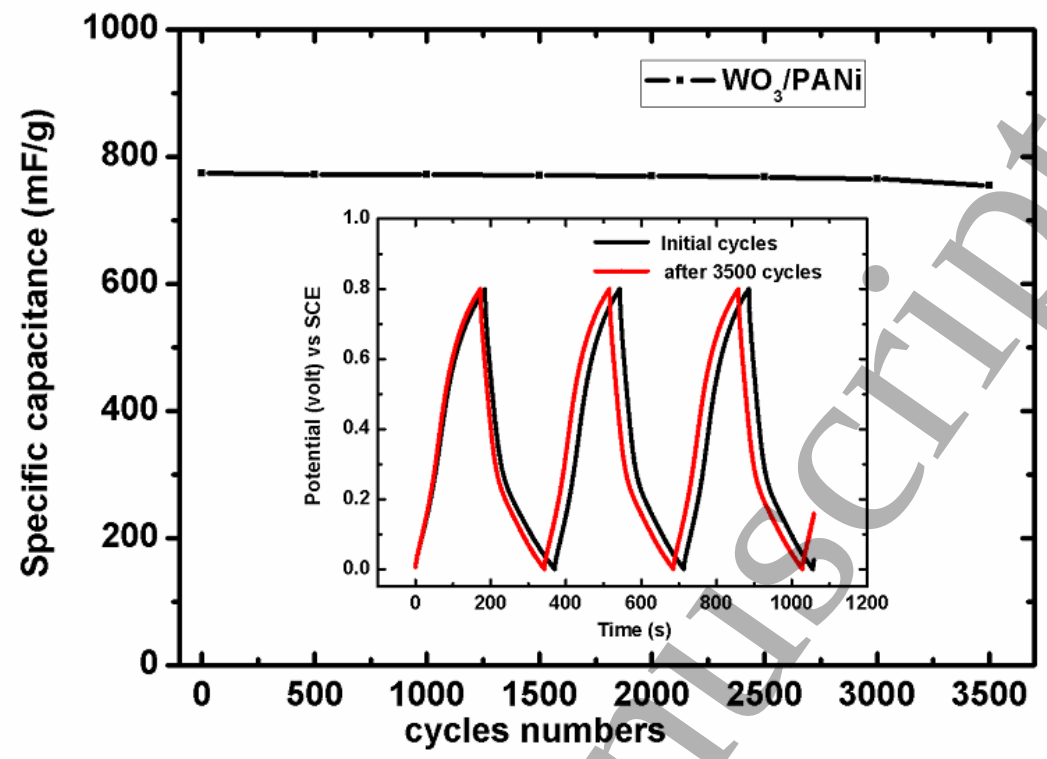

Fig. 7: Cycling stability of WO_3/PANi or initial and after 3500 galvanostatic charge/discharge (GCD) cycles in 0.5 M $LiClO_4$-PC electrolyte at constant current density 0.05 mA/cm^2

Cycling stability is a significant factor that implies effectiveness and longevity of supercapacitors. Fig. 7 illustrates the specific capacitance of WO_3/PANi film recorded for initial and after 3500 GCD cycles at a 0.05 mA/cm^2 current density. The specific capacitance increases upto 774.4 mF/g and remains stable till 3000 GCD cycles. Following this, it starts to decrease and reaches to 754.2 mF/g after 3500 GCD cycles showing less degradation (2.61%) in specific capacitance compare to earlier reports [50]. The excellent stability of WO_3/PANi could be ascribed to the concomitant performance of the hybrid material.

As a consequence, the microgloubles of PANi as a catalyst resulted in an improved morphology of WO_3 that facilitated charge storing capacity and electronic strength leading to the pseudocapacitive framework at the same time WO_3 provides its firmness to PANi with superior stability.

Conclusion

We conclude from our studies, a successful demonstration of a simple and economic aspect for the synthesis of nanocomposite WO_3/PANi film for supercapacitor application. The morphological study represented the uniform distribution of WO_3 nanodots catalyzed by PANi over the substrate and thus exhibited large surface area. The catalytic performance of PANi facilitated higher specific capacitance of WO_3/PANi with superior cyclic stability. Consequently, supercapacitor behavior of WO_3 film was improved by PANi. Synergistic effect offered by PANi enhances the surface area of WO_3. Fabricated WO_3/PANi films found to have a specific capacitance about 294 mF/cm^2 at a potential window -0.8 −0.6 V versus SCE. Thus, the present study demonstrated that the PANi globules act as a promising catalyst for WO_3 films while WO_3 provides its firmness to PANi in supercapacitor application.

Acknowledgements

The authors of this work are thankful for the financial support of DST-SERB, New Delhi for young scientist fellowship with major sponsoring of the project (grant number. PS/030/2013) and D.Y. Patil College of Engineering & Technology, Kasaba Bawada, MH, India supporting this work by developing a research lab.

References

1. A. T. Chidembo, S. H. Aboutalebi, K. Konstantinov, D. Wexler, H. K. Liu, S. X. Dou, Liquid Crystalline Dispersions of Graphene-Oxide-Based Hybrids: A Practical Approach towards the Next Generation of 3D Isotropic Architectures for Energy Storage Applications, Particle 31(2014) 465-473.

2. H. Wang, G. Ma, Y. Tong, Z. Yang, Biomass carbon/polyaniline composite and WO_3 nanowire-based asymmetric supercapacitor with superior performance, Ionics, (2018) 1-9 DOI: 10.1007/s11581-017-2428-8

3. C.J. Yuan, H.B. Lin, H.Y. Lu, Y.S. Zhang, B.Y. Xie, Anodic deposition and capacitive property of nano-$WO_3 \cdot H_2O/MnO_2$ composite as supercapacitor electrode material, Mater. Lett. 148 (2015) 167–170.

4. S.S. Thind, M. Tian, A. Chen, Direct growth and photo-electrochemical study of WO_3 nanostructured materials, Electrochem. Commun. 43 (2014) 13–17.

5. Y. Jiao, Y. Liu, B.S. Yin, S.W. Zhang, F.Y. Qu, X. Wu, Hybrid α-Fe2O3@NiO heterostructures for flexible and high performance supercapacitor electrodes and visible light driven photocatalysts, Nano Energy 10 (2014) 90–98.

6. M.J. Qiu, P. Sun, L.X. Shen, C.X. Zhao, W.J. Mai, WO_3 nanoflowers with excellent pseudo-capacitive performance and the capacitance contribution analysis, J. Mater. Chem. A 4 (2016) 7266–7273.

7. S.Yao, X. Zheng, X. Zhang, H. Xiao, F. Qu, X. Wu, Facile synthesis of flexible WO_3 nanofibers as supercapacitor electrodes, Mater. Lett. 186 (2017) 94-97.

8. J. Mao, J. Iocozzia, J. Huang, K. Meng, Y. Lai, Z. Lin, Graphene Aerogels for Efficient Energy Storage and Conversion, energy environ. sci. 53 (2018) 1-32.

9. A. Khan, A. A. Parwaz Khan, M. M.Rahman A. M. Asiri, Inamuddin, K. A.Alamry, S. A.Hameed, Preparation and characterization of PANI@G/CWO nanocomposite for enhanced 2-nitrophenol sensing, apl surface sci 433 (2018) 696-704.

10. H.Wang, M. Barrett, B. Duane, J. Gu, F. Zenhausern, Materials and processing of polymer-based electrochromic devices, mat. sci. environ. B 228 (2018) 167-174.

11. S. Patanè, C. Triolo, P. Cardiano, S. L. Schiavo, Capacitive properties of the hydrophobic [2-(methacryloyloxy)ethyl]-trimethyl ammonium nonafluoro-1-butanesulfonate poly(ionic liquid) thin film, Ionic 23 (2017) 1481-1487.

12. G.A. Snook, P. Kao, A.S. Best, Conducting-polymer-based supercapacitor devices and electrodes, J. Power Sources 196 (2011) 1-12.

13. M.O. Ansari, F. Mohammad, Thermal stability, electrical conductivity and ammonia sensing studies on p-toluenesulfonic acid doped polyaniline: titanium dioxide (pTSA/Pani: TiO2) nanocomposites, sensors &actuators B 157 (2011) 122-129.

14. J. M. Sonawane, S. A. Patil, P. C. Ghosh, S. B. Adeloju, Low-cost stainless-steel wool anodes modified with polyaniline and polypyrrole for high-performance microbial fuel cells, j. of power sources 379 (2018) 103-114.

15. S. Bhadra, D. Khastgir, N.K. Singha, J.H. Lee, Progress in preparation, processing, and applications of polyaniline, Prog. Polym.Sci. 34 (2009) 783-810.

16. H. Wang, J. Lin, Z. X. Shen, Polyaniline (PANi) based electrode materials for energy storage and Conversion, adv. mat. sci. 1 (2016) 225-255.

17. Y. Ding, S. Kan, J. Gu, J. Kan, studies on new type current collectors for polyaniline batteries, Int. J. Electrochem. Sci. 9 (2014) 6281-6293.

18. X. Li, H. Na, SPEEKK/polyaniline (PANI) composite membranes for direct methanol fuel cell usages, J. Membrane Sci. 275 (2006) 134-140.

19. K. Wang, J. Huang, Z. Wei, Conducting polyaniline nanowire arrays for high performance supercapacitors, J. Phys. Chem. C 114 (2010) 8062-8067.

20. SH Wang, CY Shen, JM Su, SW Chang, A room temperature nitric oxide gas sensor based on a copper-ion-doped polyaniline/tungsten oxide nanocomposite, Sensors (Basel). 15 (2015) 7084-7095.
21. R.Yuksel, C. Durucan, H. E.Unalan, Ternary nanocomposite SWNT/WO_3/PANI thin film electrodes for supercapacitors**,** J Alloys Comp. 658 (2016) 183-189.
22. Benxue Zou, Shengchen Gong, Yan Wang, and Xiaoxia Liu, Tungsten Oxide and Polyaniline Composite Fabricated by Surfactant-Templated Electrodeposition and Its Use in Supercapacitors, J of Nanomater. (2014) 9 pages, Article ID 813120.
23. R. Kumar, B. C. Yadav, Fabrication of Polyaniline (PANI)—Tungsten oxide (WO_3) Composite for Humidity Sensing Application, J Inorganic Organometallic Poly Mater. 26 (2016) 1421-1427.
24. H. Wei, X. Yan, S. Wu, Z. Luo, S. Wei, Z. Guo, Electropolymerized Polyaniline Stabilized Tungsten Oxide Nanocomposite Films: Electrochromic Behavior and Electrochemical Energy Storage, J. Phys. Chem. C 116 (2012) 25052−25064.
25. E. Eren, C. Alver, G. Y. Karaca, E. Uygunb, A. U. Oksuz, Enhanced electrochromic performance of WO_3 hybrids using polymer plasma hybridization process, Synthetic Metals 235 (2018) 115–124.
26. N. Asim, M F Syuhami, M. Badiei, M A. Yarmo, WO_3 Modification by Synthesis of Nanocomposites, APCBEE Procedia 9 (2014) 175 – 180.
27. C Janáky, de Tacconi NR, W Chanmanee, Rajeshwar K, Electrodeposited polyaniline in a nanoporous WO_3 matrix: an organic/inorganic hybrid exhibiting both p-and n-type photoelectrochemical activity. J Phys Chem C 116 (2012) 4234–4242.
28. Janáky C, de Tacconi NR, Chanmanee W, Rajeshwar K Bringing conjugated polymers and oxide nanoarchitectures into intimate contact: Light-induced

electrodeposition of polypyrrole and polyaniline on nanoporous WO_3 or TiO_2 nanotube array. J Phys Chem C 116 (2012) 19145−19155.

29. G.F. Samu, K. Pencz, Csaba Janaky, K. Rajeshwar, on the electrochemical synthesis and charge storage properties of WO_3/polyaniline hybrid nanostructures, J of soid state electrochemistry, 19 (2015) 2741-2751.
30. S. yao, X. Zheng, X. Zhang, H. Xiao, F. Qu, X. Wu, facile synthesis of flexible WO_3 nanofibers as supercapacitor electrodes, Materials Letters, 186 (2017) 94-97.
31. Gang Wu, Karren L. More, Ping Xu, Hsing-Lin Wang, Magali Ferrandon, Arthur J. Kropf, Deborah J. Myers, Shuguo Ma, Christina M. Johnston, Piotr Zelenay, A carbon-nanotube-supported graphene-rich non-precious metal oxygen reduction catalyst with enhanced performance durability, Chem. Commun., 49 (2013) 3291-3293.
32. G. Wu, K. L. More, C. M. Johnston and P. Zelenay, High-Performance Electrocatalysts for Oxygen Reduction Derived from Polyaniline, Iron, and Cobalt, Science, 332 (2011) 443–447.
33. Zou B-X, Liang Y, Liu X-X, Diamond D, Lau K-T, Electrodeposition and pseudocapacitive properties of tungsten oxide/polyaniline composite. J Power Sources 196 (2011) 4842–4848.
34. Nwanya AC, Jafta CJ, Ejikeme PM, Ugwuoke PE, Reddy MV, Osuji RU, Ozoemena KI, Ezema FI, Electrochromic and electrochemical capacitive properties of tungsten oxide and its polyaniline nanocomposite films obtained by chemical bath deposition method. Electrochim Acta 128 (2014) 218–225.
35. Wei H, Yan X, Wu S, Electropolymerized polyaniline stabilized tungsten oxide nanocomposite films: electrochromic behavior and electrochemical energy storage. J Phys Chem C 116 (2012) 25052–25064.

36. Tian Y, Cong S, Su W, Chen H, Li Q, Geng F, Zhao Z, Synergy of W18O49 and polyaniline for smart supercapacitor electrode integrated with energy level indicating functionality. Nano Lett 14 (2014) 2150–2156.
37. Han J, Song G, Guo R, Synthesis of Rectangular Tubes of Polyaniline/NiO Composites, J. Poly. Sci. Part A: Polymer Chemistry, 44 (2006) 4229-4234.
38. AC Sonavane, AI Inamdar, HP Deshmukh, PS Patil, Multicoloured electrochromic thin films of NiO/PANI, J. Phys. D: Appl. Phys., 43 (2010), 315102 (8pp)
39. Y. Peng, Q.G. Chen, D.Wang, H.Y. Zhou, A.W. Xu, synthesis of one-dimensional WO3-Bi2WO6 heterojunctions with enhanced photocatalytic activity, Cryst. Eng. Comm., 2015 (17) 569-576.
40. C.H.Sha, C.C. Lee, Microstructure and surface treatment of 304 stainless steel for electronic packaging, J of electronic packaging, 2011 (133) 21005-1−21005-4.
41. A.J. Bard, L.R. Faulkner, Electrochemical Methods Fundamentals and Applications, John Wiley & Sons, Inc., New York, 2001.
42. L. Qi, Z-F Li, Y. Liu, H. Zhang, Y. Ren, C-J Sun, W. Lu, Y. Zhou, L. Stanciu, E. A. Stach, J. Xie, Graphene-modified nanostructured vanadium pentoxide hybrids with extraordinary electrochemical performance for Li-ion batteries, Nature Communications, 6 (2015) 1-10.
43. Q. Wang, J-E. Moser, M. Gratzel, Electrochemical Impedance Spectroscopic Analysis of Dye-Sensitized Solar Cells, J. Phys. Chem. B, 109 (2005) 14945-14953.
44. A. E. Fetohi, R.S. Amin, R.M. Abdel Hameed, K.M. El-Khatib, Effect of nickel loading in Ni@Pt/C electrocatalysts on their activity for ethanol oxidation in alkaline medium, Electrochimica Acta, 242 (2017) 187-201.

45. D.P. Dubal, A.D. Jagadale, S.V. Patil, C.D. Lokhande, Simple route for the synthe-sis of supercapacitive Co–Ni mixed hydroxide thin films, Materials ResearchBulletin 47 (2012) 1239–1245.

46. C.J. Jafta, F. Nkosi, L. le Roux, M.K. Mathe, M. Kebede, K. Makgopa, Y.Song, D. Tong, M. Oyama, N. Manyala, S. Chen, K.I. Ozoemena, Manganese oxide/graphene oxide composites for high-energy aqueous asymmetricelectrochemical capacitors, Electrochim. Acta, 110 (2013) 228-233.

47. Ruthven DM, Brandani S, (2000) Recent Advances in Gas Separation by Microporous Ceramic Membranes, Kanellopoulos N.K. Ed., (Elsevier, Amsterdam.) p 445.

48. A.T. Chidembo, K.I. Ozoemena, B.O. Agboola, V. Gupta, G.G. Wildgoose, R.G.Compton, Nickel(II) tetra-aminophthalocyanine modified MWCNTs as poten-tial nanocomposite materials for the development of supercapacitors, Energy Environ. Sci. 3 (2010) 228–236.

49. H. Wei, J. Zhu, S. Wu, S. Wei, Z. Guo, Electrochromic polyaniline/graphite oxidenanocomposites with endured electrochemical energy storage, Polymer 54 (2013) 1820–1831.

50. R. Yuksel, C. Durucan, H. E. Unalan, Ternary nanocomposite SWNT/WO3/PANI thin film electrodes for supercapacitors, J. Alloy Compd. 658 (2016) 183-189.